Journal of Microelectronics and Electronic Packaging (2023) **20**, 17–26

ISSN: 1551-4897

Prevention of Cu Electrolytic Migration Defects on RDL by a Cu-Selective Passivation to Enhance Reliability

Ashish S. Salunke,* John Alptekin, Kaushik Akula, Subiksha Jayakumar, Shaurya Kumar, and Oliver Chyan

***Abstract*—Copper (Cu) is the metal of choice for the redistribution layer (RDL) to facilitate fast I/O communication in an integrated circuit (IC). Cu can electrochemically migrate (ECM) between the array of electrodes under bias, electrolyte, and moisture. IC packages fail miserably when exposed to various ion impurities and moisture. Copper at the anode dissolves to form Cu^{+1} and Cu^{+2} ions. As the anodic dissolution continues, the concentration of copper ion increases. These anions deposit on the cathode leading to Cu dendrite formation. To achieve the near-zero parts per billion defectivity goal, elimination of ECM defects in packaged devices is critical. This work discusses the development of a novel Cu-selective passivation and a method to accelerate reliability testing. A hydrophobic passivation with minimum stress to the IC package is proposed in this work. The new passivation coating is thermally stable, strongly adheres to Cu, is corrosion resistant, low cost, and shows good potential to prevent ECM defects. The coated packaged devices were tested by an accelerated PEG drop test (PDT) to explore its ECM prevention capabilities.**

***Keywords*—Wafer-level package, ECM, reliability, passivation, PEG drop test, metrology**

Introduction

Advances in the fabrication process of integrated circuit (IC) aim for faster and less expensive electronics [1]. Automotive engines working under extreme temperature and humidity are the major consumers of these electronics [2]. Electronic industry demands a low-cost and high-performance packaging technology [3]. Recently, IC packaging processes have been developed on wafer level [4]. Wafer-level package (WLP) comprises of mainly redistribution layers (RDL), under bump metallization (UBM), primary and secondary passivation layers, and underfill material (epoxy molding compounds). RDLs are made up of metals due to their electronic, mechanical, and magnetic properties [5]. However, corrosion/migration-related reliability issue can affect the mechanical and electrical properties of RDL metals used in WLP [6].

Copper has better thermal and electrical properties. It is the choice metal for RDL on the Si die. Typically, a polyimide passivating film is conformally coated on the Cu RDL due to its good insulation and mechanical properties. A polyimide film isolates the Cu from exposure to the atmospheric contaminant [7]. The coefficient of the thermal expansion (CTE) for these components are Si die (∼2.6 ppm/°C), Cu (16.5 ppm/°C), and polyimide (35.9 ppm/°C) [8]. When exposed to high temperature and humidity, the wafer can potentially undergo delamination and cracks due to the CTE mismatch. Also due to the resistive joule heating of the microelectronics, the temperature inside the IC package can rise up to 250°C [9]. Such delaminated wafers when exposed to the humidity lead to further reliability consequences. It is well documented that water lowers the glass transition temperature (T_g) of the polymer as it is acts as a plasticizer [10]. Above T_g, the free volume of the dielectric is increased, and its bond strength and the stiffness are decreased [11]. The increased free volume and the reduced bond strength with water absorption leads to a localized microchannel containing high level of moisture within the build-up dielectric [12]. This, in combination with the applied electric field, provides a means for an electrochemical migration (ECM).

ECM is defined as the transport of metal ions from the anode and deposit at the cathode through an electrolyte medium. The electrochemical processes involved here are electrolytic decomposition and metal migration [13, 14].

As illustrated in Fig. 1 the anodic copper dissolves to form Cu^{n+} ions and releasing n electrons.

$$Cu \rightarrow Cu^{n+} + ne^{-}$$

As the anode dissolves, the generated copper ions migrate toward the cathode and is reduced and deposited as the seed layer of Cu that cumulates into dendrite growth with time.

$$Cu^{n+} + ne^{-} \rightarrow Cu$$

Ionic contaminants act as a supporting electrolyte in an electrochemical process and have an important impact on ECM. Contaminants like perchlorates, sulfates, chlorates, nitrates, and chlorides are found more significantly in the microelectronic package [15]. Ionic contaminants increase the conductivity of the electrolyte, thereby increasing the rate of the ECM failure. In the presence of humidity and such aggressive ions, Cu RDL–patterned interconnects are susceptible to ECM under biased conditions. This type of failure possibility is relatively new for chip-level interconnections, since the previously used aluminum, gold, and tin was less susceptible than Cu RDL to ECM defects [3, 16, 17]. A device operating properly for hundreds of hours under ideal conditions might undergo failure immediately after exposure to corrosive environmental conditions. The expenses incurred due to the failed electronic component is

The manuscript was received on January 8, 2023; revision received on February 12, 2023; accepted on February 23, 2023.

The original version of this article was presented at the 55th International Symposium on Microelectronics (IMAPS'2022) in Boston, MA on October 4–6, 2022.

Interfacial Electrochemistry and Materials Research Lab, University of North Texas, Denton, Texas

*Corresponding author; email: ashishshivajisalunke@my.unt.edu

doi:10.4071/imaps.1903845

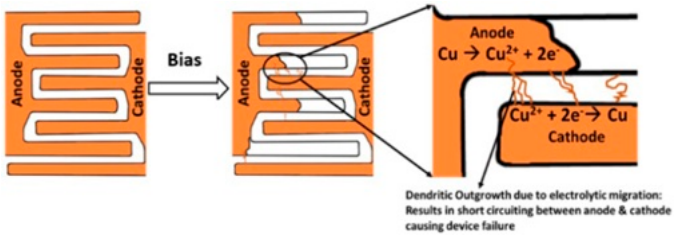

Fig. 1. Mechanism of electrochemical migration of Cu in water medium under bias.

far larger than compared with the cost of the failed components itself.

To enhance the ECM resistance, various surface finish options have been reported. Immersion silver (ImAg), electroless nickel immersion gold (ENIG), and electroless Ni have been reported [18, 19]. Topper et al. focused on conformal coating such as polyurethane, acrylic, epoxies, and silicones and its properties were tested from the packaging point of view [20]. Special semiconductor-grade polymers have been developed as passivation layers. Polyimides and benzocyclobutane (BCB) are standard passivation layers for memory chips and devices [7, 21]. The process of coating these polymers typically involves a rather high curing temperature and includes multiple steps [21]. Therefore, there is a need to develop an alternative passivation coating, for preventing ECM failures, which is Cu-selective with low moisture retention and lower stress and can be deposited at relatively lower temperature.

To evaluate lifetime reliability, IC packages routinely underwent thermal stress test following JESD22-A110 standards (130°C, 85% RH for 96/256 h) with or without bias [22]. However, this test is time consuming to evaluate the performance of passivation coating for ECM failure as it corresponds to short circuit failure time. An accelerated and simpler screening testing method will be helpful for initial quick screening of the passivation coatings efficiency. Some reports have suggested that the water drop test (WDT) as a candidate of acceleration test [23-25]. However, when the spacing between the electrodes is only a few microns, the rate of ECM is too fast to be studied by WDT. Carbone and Corl developed an accelerated test to study ECM in polyethylene glycol (PEG-400) media that is much less conductive than water [15, 26]. PEG drop test (PDT) was performed by doping the PEG-400 with ionic contaminants to simulate ECM defect–forming condition. This method of screening, when paired with a microscope, helps to find the pinholes in the coating and reveals any localized surface defects [27, 28].

In this report, we provide new results of developing a novel passivation coating for Cu RDL and utilize PDT screening test and other characterization tools to evaluate its ECM protection ability. The initial work was centered on detailed PDT failure analyses of the high-density Cu RDL devices with spacing of 8, 10, 14, and 18 μm immersed in PEG with added contaminants like SO_4^- and ClO_4^-. Real-time PDT was conducted to analyze the migration behavior between the arrays of Cu electrodes within an applied potential window, and scanning electron microscopy/electron dispersive x-ray spectroscopy (SEM/EDS) analysis was used for elucidating the dendrite morphology and composition. Then, the Cu RDL devices were coated with a new Cu-selective passivation layer and subjected to the same PDT test for comparison. We utilized electrochemical tools (potentiodynamic polarization and linear swipe voltammetry [LSV]) combined with contact angle measurements, Fourier transform infrared spectroscopy (FTIR), and SEM/EDS to evaluate the passivation nature of the Cu-selective coating.

Materials and Experimental Method

Cu RDL test devices were fabricated on an Si substrate containing four different spacings: 8, 10, 14, and 18 μm as illustrated in Fig. 2. These Cu RDLs can be connected to the external circuit by the Al wires, which were ball bonded onto the Cu UBM. The RDL test chips were mounted on a ceramic dip package for the ease of handling and testing. PEG-400 doped with either 1,000 ppm SO_4^{2-} or 100 ppm ClO_4^- was prepared from ACS-grade chemicals of Na_2SO_4 and $KClO_4$ [29]. These solutions were stored in an airtight container due to the hygroscopic nature of PEG-400 [30].

The Cu array electrodes were coated by a versatile, thermally stable, and economically effective inhibitor by a single-step chemical vapor deposition (CVD) at temperatures as low as 100-200°C [31]. The composition and selectivity of the coating is studied by SEM. To test the coating's ability to prevent ECM, LSV electrochemical characterization was performed on sputtered Cu on Si wafer (with and without coating) utilizing CHI 760D potentiostat. The sputtered Cu wafers and platinum electrodes were used as working and counter electrodes, respectively. Saturated Ag/AgCl electrode was used as the reference electrode. LSV was performed from −0.1 V to 2 V (vs. Ag/AgCl) at a scan rate of 10 mV/s using the abovementioned three-electrode system in 3.5% NaCl. This solution is used because that was one of the most reported solutions used for studying severe Cu corrosion. Potentiodynamic polarization was performed on the same samples at 1 mV/s.

After the preliminary screening of the passivation coating on the Cu wafer, PDT was conducted to understand the ECM failures on the coated and the uncoated device. To establish a benchmark for the ECM testing of the Cu RDL, PDT was used. Nonaqueous PEG matrix was doped with ions (ClO_4^-, SO_4^{2-}) to simulate an EMC environment (Epoxy molding compounds). The real-time changes on Cu RDLs immersed into a contaminant-spiked PEG-400 solution with applied bias were observed under optical microscope paired with a camera. ECM is tested on the Cu RDL patterns with a line to line spacing (L:S) in submicron range. The successful biased PEG-400 immersion test outcome on the test devices helped to guide the choices for the most promising passivation layer for subsequent molding and the more time-consuming biased highly accelerated stress test (BHAST) testing.

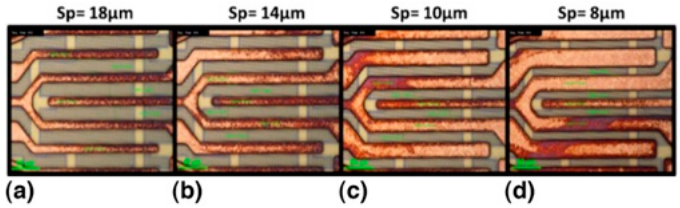

Fig. 2. (a-d) 8-18-μm spaced Cu RDL electrodes.

A 30-μL droplet of the different solutions, i.e., (1,000 ppm SO_4^{2-} and 100 ppm ClO_4^-) doped in PEG-400 were added between the array of electrodes. All micro electrochemical experiments were conducted using a potentiostat, CH Instrument 760D. Leads for both auxiliary and reference electrodes from the potentiostat were connected to the anodic Cu RDL array, and the working electrode lead to the cathodic RDL array. The preset voltage was applied across these interdigitated RDL array electrodes by the potentiostat with a scanning rate of 10 mV/s. While the resulting *I-V* plot was collected, the ECM defects formation was monitored concurrently by a Nikon LV150N Metallurgical microscope, as illustrated in Fig. 3. Thus, the PDT setup captured the leakage current due to the ECM dendrite during the potentiodynamic polarization as a function of time/potential until a permanent short circuit was observed.

The FEI Nova 200 Nano Laboratory SEM was employed to analyze the surface morphology of the tested devices and its elemental composition via EDS. The chemical bonding of the passivation layer was analyzed using a Thermo Scientific Nicolet iS-50 FITR spectrometer equipped with a spectra-tech specular reflectance accessory (Vee Max II). The CVD-coated Cu wafer was analyzed immediately after the deposition without further treatment. The thermal stability of CVD passivation coating was studied by thermal gravimetric analysis (TGA) using Q-50 thermogravimetric analyzer.

Results and Discussion

A. Accelerated Reliability Testing of Cu Redistribution Layers

Results of the ECM behavior of Cu RDL electrodes on WLP test samples in accelerated testing solution, i.e., 1,000 ppm SO_4^{2-} and 100 ppm ClO_4^- are presented below. The chosen concentrations are the maximum solubility limit of these ions in PEG-400 [32]. To investigate the ECM resistance behaviors of Cu electrodes, anodic polarization tests were conducted to obtain *I-V* curves. This investigation shows the aggressive dendrite formation with the decrease in the spacing between the electrodes and provides useful insight of the critical failure regions on the RDL. The resulting base current variation for each Cu RDL device can be correlated to the short-circuit events caused by ECM between the interdigitated array electrodes.

Fig. 4 shows two captured images of Cu RDL arrays from real-time monitoring of ECM process in 100 ppm ClO_4^-/PEG-400

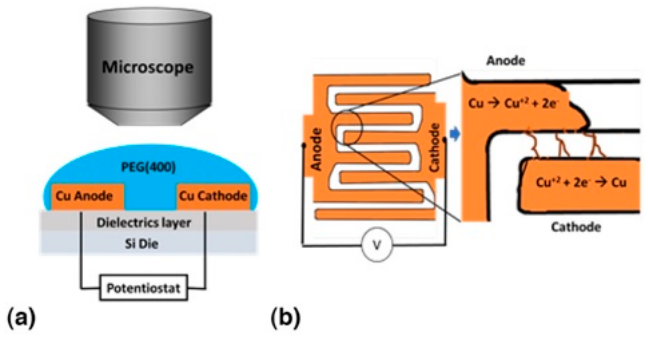

Fig. 3. (a) Illustration of PEG drop test (PDT) screening metrology setup. (b) Top view of the dendrite formation.

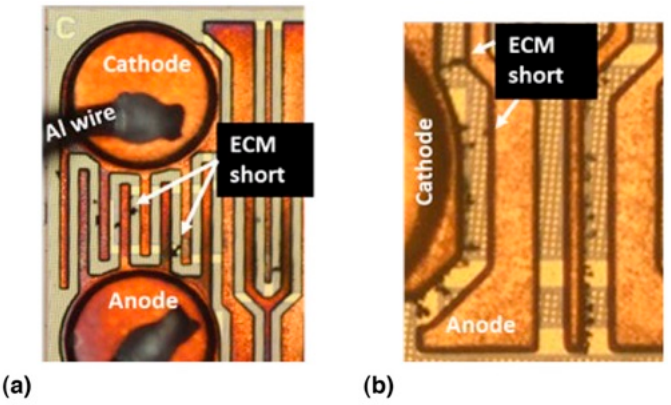

Fig. 4. Real-time monitoring of the ECM short-circuit events captured by microscopic images (a) under ~3-V bias in 100 ppm ClO_4^- + PEG-400 and (b) under ~2-V bias in 1,000 ppm SO_4^{2-} + PEG-400.

and 1,000 ppm SO_4^{2-}/PEG-400. Both RDLs have the interelectrode spacing of 10 μm. An increase in the positive potential leads to the oxidation of the Cu anode electrode. The Cu ions from the anode begin to migrate to the Cu cathode. These migrating Cu ions deposited on the Cu cathode forms Cu dendrite that naturally grow toward the anode, where the concentration of Cu ions will be the highest. When cathodic dendrites eventually reach the anode in the RDL device, short-circuit current abruptly increased due to the conductive pathway formed between interdigitated RDL electrodes. This thin dendritic conductive pathway quickly broke down under the applied potential and current density, and gave rise to the "spike" shapes in the *I-V* plots (Fig. 5). Consequently, Cu dendrites can be observed on both cathodic and anodic electrodes in Fig. 4. The real-time imaging of short-circuit events can potentially allow PDT screening to identify the potential ECM vulnerabilities originated from specific RDL design and materials makeup.

Fig. 5a shows the *I-V* plots on Cu RDL electrodes with different interelectrode spacings submersed in 100 ppm $KClO_4$ of PEG-400 solutions. As the ECM reaction proceeded continuously with increasing positive bias, caused more dendrite bridging and short-circuit current spikes due to the nonterminating source of copper ions. The *I-V* plots reveal that the onset potential for the short-circuit event from the bridging Cu dendrite increased with the increase in the spacing between the Cu electrodes. Based on the in situ monitoring video, a very thin dendrite network was formed between the 8-μm spaced electrodes at 2.8 V, which was sensed by the spike in the current as illustrated in Fig. 5a. Onset of the first current spike is observed at increased bias with increased spacings, that is, 10 μm (3.1 V), 14 μm (3.55 V), and 18 μm (4.3 V). The number of current spikes increase with the decrease in the spacing of the electrode. This reveals that spacing is a critical factor in the ECM failure. The dendrites formed were generally thinner and covered the surface of the electrode.

In Fig. 5b, the effect of sulfate ion, another major potential contaminant, on Cu RDL test samples was carried out. Since the concentration of the sulfate ion was 10 times higher than the perchlorate ion, more ions were available for the ionic mobility of the ionized Cu ion in the solution. As shown in Figs. 5a and 5b, the onset potential for the short-circuit current

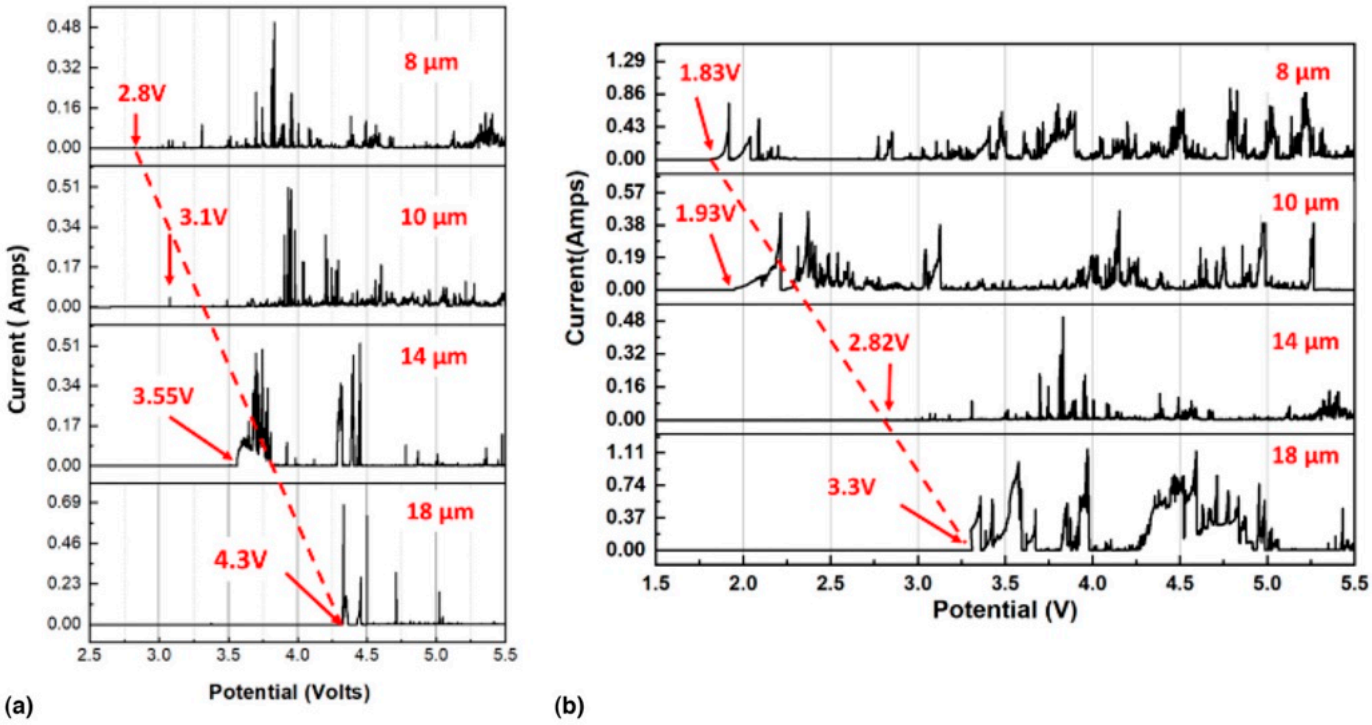

Fig. 5. (a) *I-V* plots of the ECM short-circuit events under (0-5.5 V) bias in 100 ppm ClO_4^- + PEG-400. (b) *I-V* plots of the ECM short-circuit events under (0-5.5 V) bias in 1,000 ppm SO_4^{2-} + PEG-400.

spikes in 1,000 ppm sulfate ion is lower as compared with 100 ppm perchlorate. The dendrite formation initiated at 1.83 V for the 8-µm spaced electrodes. Similarly, for the 10-µm spaced electrodes, the dendrite formation initiated at 1.93 V. With an increase in spacing by 4 µm, the initiation voltage shifted to 2.82 V for the 14-µm spaced electrodes. Similar effect is seen upon further increase in the spacing by another 4 µm leading to a short at 3.3 V for 18-µm spacing of the electrodes. The results generated from this PDT test support its potential application as an accelerated screening test on the passivation coatings to prevent ECM defects, then confirmed by the more rigorous BHAST.

When a higher positive potential (>10 V) was applied to Cu RDL electrodes arrays, massive electric shorts can form and lead to a permanent failure of the device. Fig. 6a shows the SEM image of a failed RDL device after PEG drop test in perchlorate solution. Dendrites are broadly evident in the image, and it grows because of dissolution of the anode, which further fringes toward the cathode. Dendrites formed between the array electrodes can be identified as trunk, lace-type dendrites, and sludge. A single dendrite bridging within the electrolyte is a trunk-type dendrite. The lace-type dendrites grow on the inside surface of the electrode. Sludge develops when the dendrites between the two electrode serves as the pathway for high current flow, thereby burning the individual dendrites. The dendrite microstructure shown in the image reveals dendrite branching out in multiple directions. The massive dendrite formation can overcoat the entire cathode contact pad and contact wire. It is observed by EDS mapping in Fig. 6b, that the dendrites were made up of Cu oxidation forming CuO_x. This conclusion leads us to another major aspect of this work, which focuses on the prevention of these accelerated ECM reactions on Cu RDL interconnects under high potential bias by applying a new hydrophobic passivating layer.

B. Application of Passivation on the Cu Redistribution Layers

The main role of the passivation coating is to minimize or completely negate the dissolution of Cu when encountering ECM-favorable condition during the operation lifetime of a packaged device. A rigid, dielectric/polymeric passivation coating could add additional stress to cause unwanted wafer warpage due to CTE mismatch. Recently, we have developed a novel patent-pending method of depositing an organic passivation coating on Cu surface [31]. As shown in Fig. 7, the passivation coating is highly Cu-selective—only deposited on Cu RDL features. No coating was observed on other metals, inorganic dielectrics, and polymers used in the typical packaging devices. Therefore, the new passivation coating selectively deposited only on Cu RDL interconnects should, in principle, generate less stress compared with the currently used blanket coating of dielectric or polymeric coatings. As described in the various characterization outcomes below, the new coating has a hydrophobic surface, thereby preventing moisture from reaching Cu surface to initiate ECM reactions and the above-described chain events leading to the ECM failure. Additional advantages of the new passivation coating are low cost, compatible to current packaging operation, and thermally stable up to 250°C.

C. Accelerated Reliability Testing of Cu Redistribution Layers After Passivation

The passivated Cu RDLs are tested by the PEG drop test. The passivated Cu RDL were anodically swept from 0 V to 10 V.

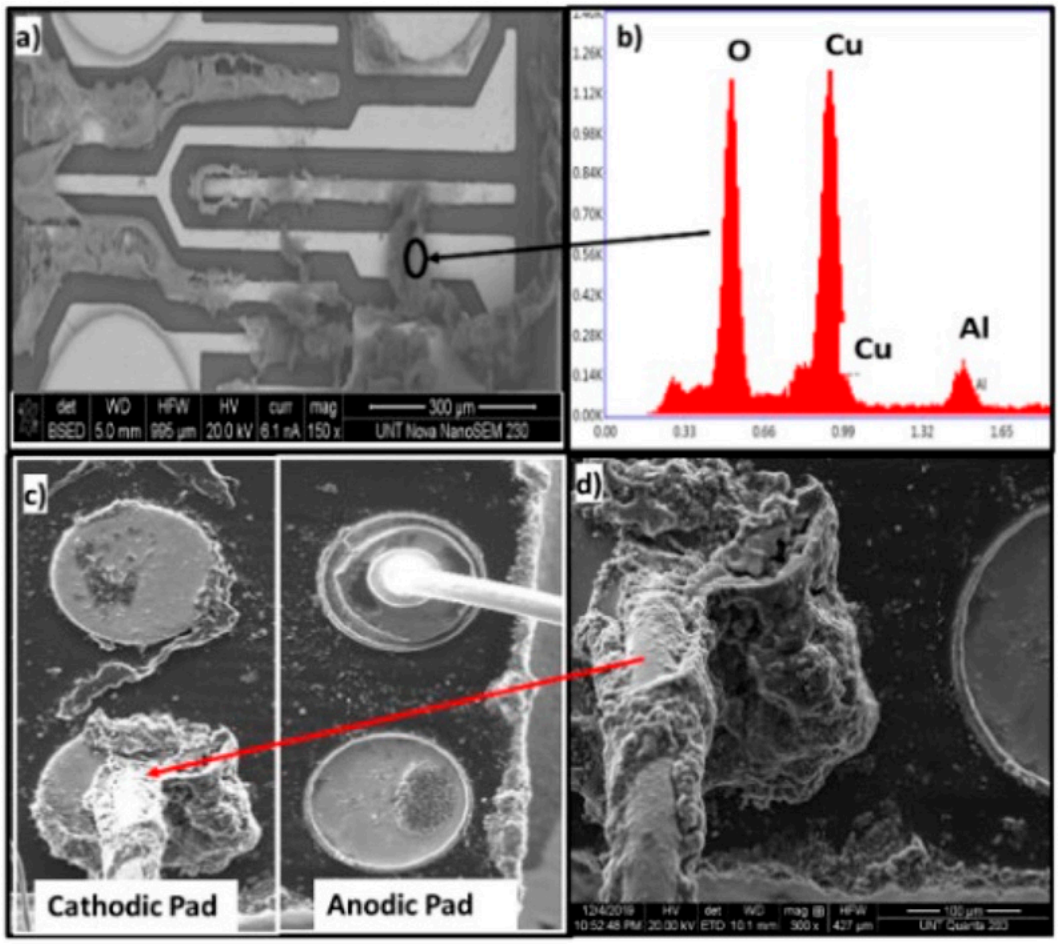

Fig. 6. SEM image showing the (a) trunk-type dendrite formation, (b) EDS reveals that CuO_x is the main constituent of the dendrite, (c) Cu electrodeposited on the cathodic pad and dissolution on anodic pad, and (d) zoomed-in image of the cathodic pad showing dendrite formation.

As seen in the *I-V* plots of Fig. 8a, even with a much higher positive potential bias of 10 V, there is complete absence of current spikes in the passivated Cu RDL as compared with the nonprotected bare Cu RDL (Fig. 5). Therefore, Cu-selective passivation coating completely prevents any ECM-related short-circuit events, when immersed in a PEG media doped with a maximum ion concentration of sulfate or perchlorate. As shown in Fig. 8a, a slow increase of small background (<10 μA) was observed in the PDT test. This background current value compared with the current spikes of uncoated Cu RDL, was 200 times less. We attribute this slow rise of background current to the capacitive charging of interdigitated RDL electrodes immersed in the PDT test solution. This assertion is consistent with the observed higher background currents with a smaller RDL interelectrode spacing.

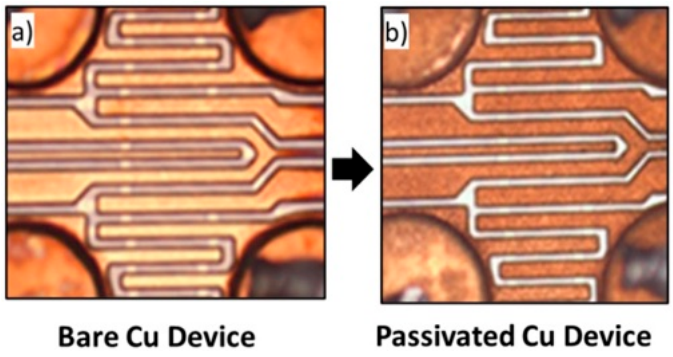

Fig. 7. (a) Bare Cu device and (b) CVD-passivated Cu device.

Based on the SEM image in Fig. 8b, the coated Cu RDL remained intact with no observation of dendrite formation after positive 10 V bias of the PDT screening test. The coated film is not tarnished even after the long exposure to the corrosive environment under positive potential bias. This can be attributed to the strong adhesion of the coating to Cu and its high hydrophobic surface, (see Section E Fig. 12) to repel moisture. These results indicate that the passivation coating can prevent electrochemical migration. Fig. 9 shows the direct comparison of the bare Cu device with the coated Cu device. The current scale on the bare Cu device is in milli amps range whereas on the coated Cu device it is in micro amps range. It can be confirmed by this comparative analysis that the inhibitor-coated device is capable of preventing the electrochemical migration failure of the device.

D. Electrochemical Characterization Studies of Passivation on Blanket Cu Wafer

To further evaluate the passivation strength of Cu-selective coating, blanket Cu wafer samples with/without coating were

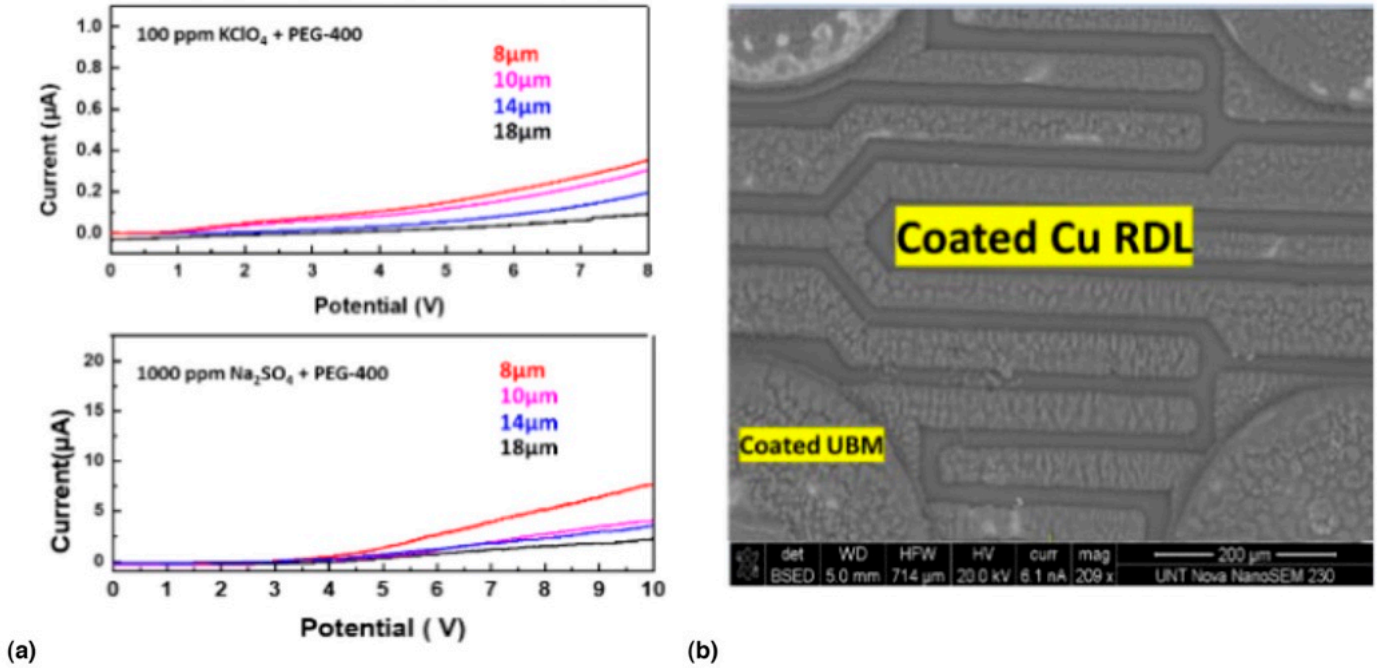

Fig. 8. PEG drop test on coated Cu RDL in (a) 100 ppm ClO_4^- and 1,000 ppm SO_4^{2-} and (b) SEM image of 8-µm coated RDL device after PDT test.

subjected to a highly corrosive environment of 3.5% NaCl solutions. If the passivation can survive this extreme corrosion environment it should be effective in normal use in IC-package condition. Fig. 10 shows the polarization curves of coated and bare copper wafer in 3.5% NaCl solutions. The most important property of the passivation coating is its ability to prevent the oxidation of the underlying Cu surface. Electrochemical parameters like corrosion potential (E_{corr}), corrosion current (I_{corr}), and efficiency of inhibition (η%) were calculated from the polarization curve. The corrosion rates of coated and the blanket Cu were compared by the potentiodynamic polarization test.

In the absence of passivation coating the corrosion potential of Cu was $E_{corr} = -0.23$ V, which was more negative than the corrosion potential for the coated Cu substrate sample ($E_{corr} = 0.35$ V). This shows that higher positive potential is required to break down the passivation coating on the Cu surface. The corrosion current density of bare Cu in 3.5% NaCl solution ($I_{corr} = 9.4$ µA/cm^2) was about 4,100 times higher than that observed for a passivated Cu surface ($I_{corr} = 2.3$ nA/cm^2). The corrosion rate was also found to drop from 60 Å/min without protection to about 1 Å/min after passivation coating. Therefore, the observed potentiodynamic polarization confirms that the passivation can prevent the Cu surface from severe oxidative corrosion in a highly corrosive 3.5% NaCl solution.

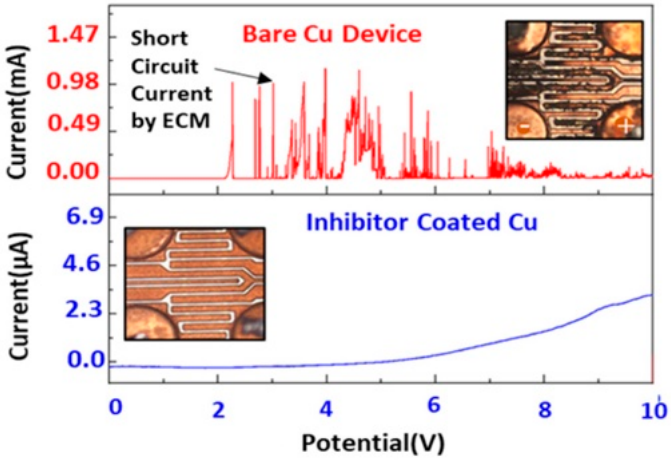

Fig. 9. Comparison of the *I-V* plot between the inhibitor-coated RDL device and the bare Cu RDL device.

Fig. 10b presents an LSV of a blanket and coated Cu substrate in 3.5% NaCl solution. The LSV was collected by scanning from negative to positive potentials (anodic scan) with a scan rate of 10 mV/s. The anodic peaks were observed at 0.03 V and 0.89 V along with a satellite peak at 0.5 V corresponding to Cu (0) to Cu(I) and Cu(I) to Cu (II) oxidation, respectively. The blanket Cu surface was corroded readily in 3.5% NaCl solution. In contrast, the passivated Cu surface showed negligible oxidation current from multiple LSV scans from open circuit potential to 1.2 V. The observed oxidation prevention of Cu is mainly attributed to the hydrophobic nature of the film and the bonding strength of the chemisorbed passivation film on Cu surface.

E. Material Properties of Passivation Coating

The passivation coating is highly selective to Cu over any other materials on the packaging device. The thermal stability was studied by FTIR and TGA. Fig. 11 shows the FTIR spectra of passivation coating with a highlighted sp^2 hybridized C–H bond stretching mode at 3,064 cm^{-1}. After annealing in 260°C for 30 min, the intensity of the characteristic bonding features

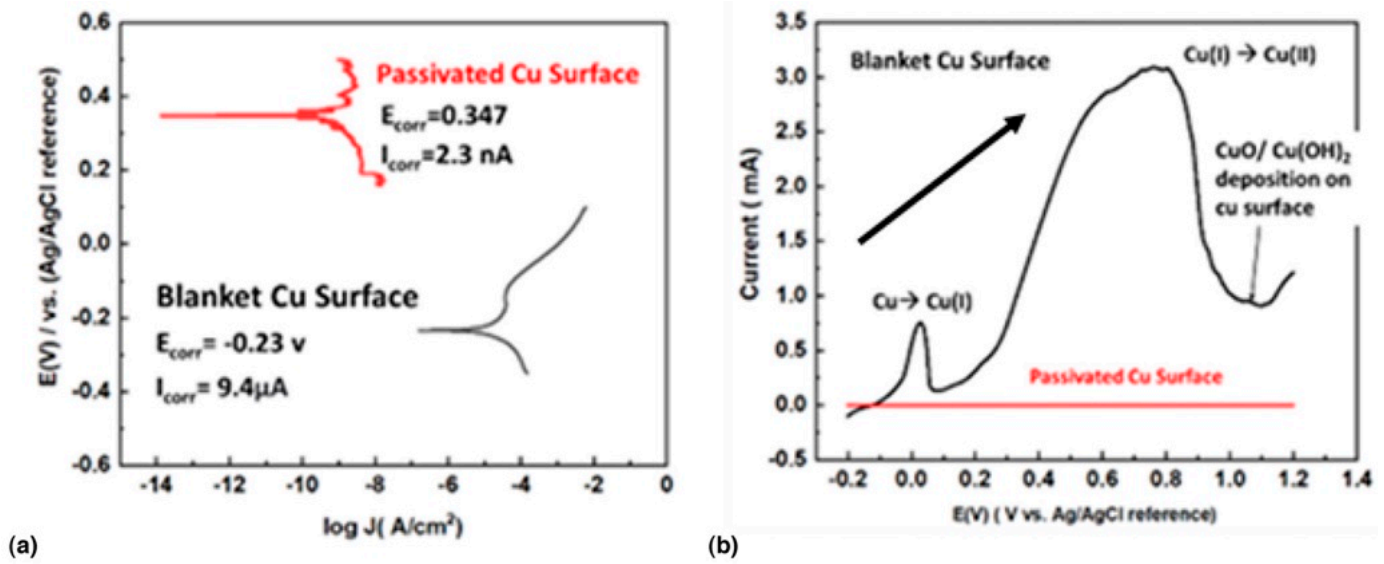

Fig. 10. (a) Tafel plot analysis of Cu with/without passivation in 3.5% NaCl. The scan rate used is 1 mV/s. (b) Linear sweep voltammogram of Cu electrode with/without passivation in 3.5% NaCl. The scan rate used is 10 mV/s. (Use straight arrow in Fig. 10b.)

was found to be unchanged in terms of its peak distribution and peak height showing the high thermal stability of the coated layer and its potential compatibly with IC packaging processing flow.

Due to the development of reflow solder process, the soldering in the surface mount technology involves exposing the packaging devices to temperatures as high as 220–260°C. So, the Cu wafer surface with coated passivation was artificially exposed to a higher temperature of 260°C for a period of 30 min to study the thermal stability. The passivation has a high decomposition temperature, which was confirmed by TGA. As shown in Fig. 11b, there is an initial loss of 20% originated from physiosorbed material from the Cu surface. After 210°C, the passivation coating is very stable until 350°C. No chemical bonding signature changes observed after 260°C annealing from Fig. 11a also support this assessment.

Fig. 12a shows the water wettability measurement of Cu-selective passivation coating that exhibits a high hydrophobicity with water contact angle of 132°. Due to this hydrophobic nature of the coating deposit, the moisture retention on the film is very low that helps to prevent Cu oxidation in a highly corrosive environment. The surface topography changes of the Cu after coating can be seen by the SEM/EDS in Fig. 12b. The focused ion beam-SEM imaging observed at 20Kx magnification revealed that the CVD coating process creates a blanket coating on the Cu surface. The thickness of the coating was found to be ~400 nm. Since the coating is Cu selective, it can cover all exposed Cu surface of a Cu RDL device. Thus, the passivation coating can enclose the Cu RDL interconnects from all the dimensions to form a conformal hydrophobic layer to provide an excellent barrier against potential ECM defects.

F. Investigation of Polyimide Coating and Its Electrochemical Migration Failure

Packaging industry relies on polyimide as a passivation layer for the Cu RDL. Such passivated devices were investigated by PDT to reveal the weak spots on the RDL prone to electrochemical migration failure. Polyimide coating on copper is prepared by spin coating followed by thermal annealing. During spin coating, it is possible that some of the regions on the Cu

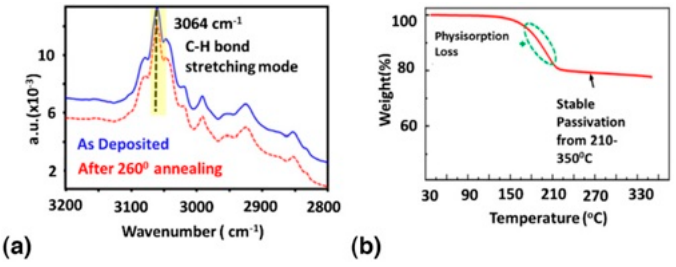

Fig. 11. (a) Reflectance infrared spectra of the passivation film as deposited (blue) and after 260°C annealing (red). (b) TGA analysis of the passivation coating powder obtained from Cu surface.

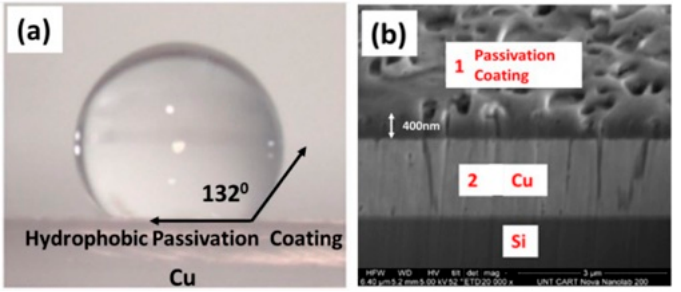

Fig. 12. (a) Water contact angle and (b) FIB-SEM cross-section image of the passivated Cu RDL.

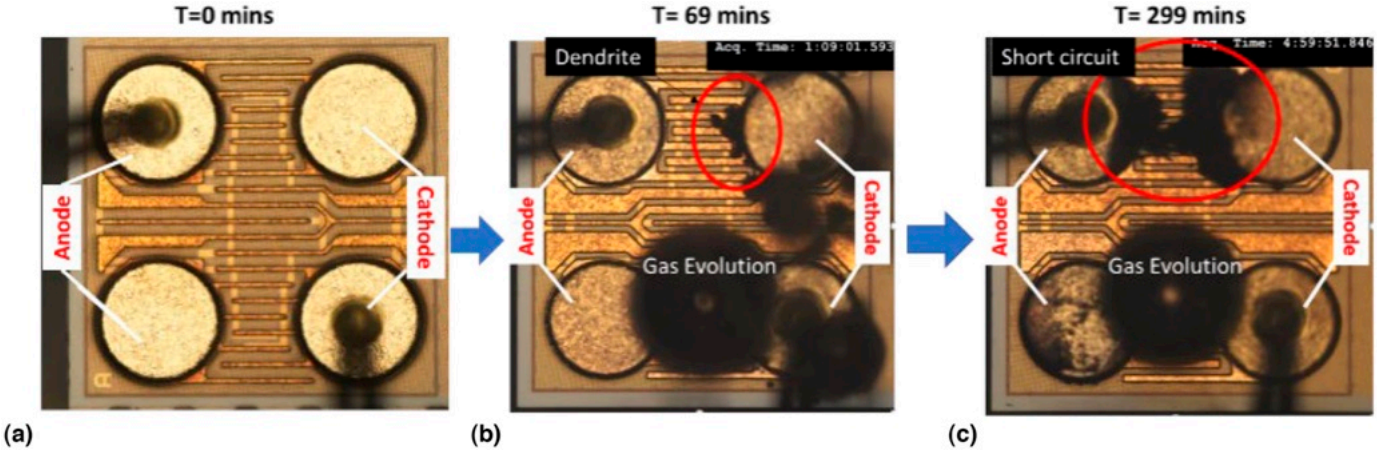

Fig. 13. PDT on polyimide-coated Cu RDL in 100 ppm $KClO_4$ + PEG-400 solution (a) T = 0 min, (b) T = 69 min, and (c) T = 299 min.

RDL remain uncoated. These uncoated regions can be the weak spots for dendrite formation, thereby leading to a short circuit caused by electrochemical migration of Cu. Fig. 13 illustrated the time-dependent evolution of dendrite formation tested in 100 ppm $KClO_4$ at 10 V. Microscope image was recorded before PDT and also during the experiment. After 69 min of PDT, Cu ion deposited at the cathode, can be seen migrating toward the anode. Gas is also evolved at the cathode. After 299 min, it is observed that the dendrites connected between the anode and cathode. At this point, the device fails by short circuit. The spacing between the two Cu UBM is 100 μm and the electrochemical migration rate of the Cu ion in 100 ppm $KClO_4$ solution is 0.33 μm/min. Weak spot was observed only at the interface of the Cu UBM and the Cu RDL. This device can be prevented from ECM failure by CVD of passivation coating at the interface. However, it is industrially noneconomical to coat the Cu RDL first with polyimide and follow with another passivation coating. A one-step solution can be used to replace the polyimide coating with the passivation coating developed by CVD.

A microscope image–based comparison between bare Cu, polyimide-coated Cu, and the CVD passivation coating on Cu RDL was done to comment on the efficiency of each method to prevent the ECM. Fig. 14 presents the microscope images tested by PDT in 100 ppm $KClO_4$ + PEG-400 solution at 10 V. Bare Cu device was damaged by developing a short between the two electrodes and due to the resistive joule heating, the Cu electrodes melted or warped. In the polyimide-coated device, the dendrite was connected through the interface of the Cu UBM and RDL. This dendrite network is weak as compared with the bare Cu; hence no severe short-circuit damage is observed. However, this dendrite connection is still substantial from the I/O signal loss point of view. Inhibitor-passivated Cu RDL substrate showed in Fig. 14c exhibited excellent ECM protection as discussed earlier. Negligible dendrite formation was observed on these devices. As this passivation coating is selective to Cu, there is less concern of the warpage of the WLP due to CTE mismatch.

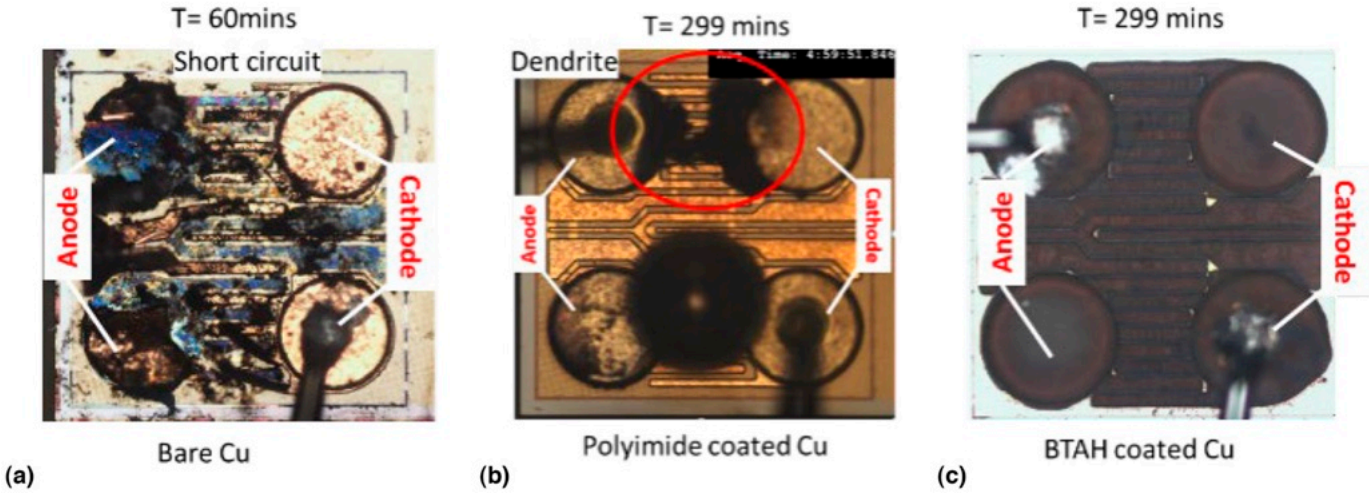

Fig. 14. PDT comparison for (a) bare Cu, (b) polyimide-coated Cu, and (c) passivation-coated Cu in 100 ppm $KClO_4$ + PEG-400 solution.

Conclusion

Real-time accelerated PDT screening reveals a trend of onset potentials for short-circuit events resulted from bridging dendrite formed by ECM between the Cu RDL interconnects. From this correlation, it can be concluded that surface passivation, electrode spacing, applied bias, and ionic contaminants are all major factors for ECM failure. The bare Cu system will corrode/damage immensely at higher bias and the passivated Cu RDL will not damage severely after testing with accelerated PDT. PDT helps to identify the critical factors contributing to the ECM failure. Visibly uniform, ultrathin, and conform coating on the Cu RDL prevents the dendrite formation and severe damage of the Cu RDL on the WLP device. Surface passivation coating makes the surface hydrophobic, thereby, further preventing RDL from the risk of ECM failure. Major advantages of the coating are that it is selective to copper surface. The coating is robust and thermally stable up to 260°C. The passivation coating process is low cost and compatible to the current packaging operation.

Acknowledgments

The work upon which this article is based was supported by Texas Instruments and University of North Texas. The assistance of Joshua Caperton with the SEM/EDS measurements is acknowledged. The authors thank Luu Nguyen and Thu Tran from TI for providing test samples for this work.

References

[1] R. Ghaffarian, "Microelectronics packaging technology roadmaps, assembly reliability, and prognostics," *Facta Universities. Series: Electronics and Energetics*, Vol. 29, No. 4, pp. 543-611, 2016. https://doi.org/10.2298/fuee1604543g.

[2] M.E. Stahley and J.W. Osenbach, "Copper migration in flip-chip substrates under biased-HAST conditions," *Additional Conferences (Device Packaging, HiTEC HiTEN, and CICMT)*, Vol. 2011, No. DPC, pp. 002465-002480. https://doi.org/10.4071/2011dpc-tha35.

[3] G. Harsanyi, "Copper may destroy chip-level reliability: handle with care-mechanism and conditions for copper migrated resistive short formation," *IEEE Electron Device Letters*, Vol. 20, No. 1, pp. 5-8, 1999. https://doi.org/10.1109/55.737556.

[4] C.-H. Lu, Y.-T. Kho, Y.-T. Yang, Y.-P. Chen, C.-P. Chen, T.-T. Hung, C.-F. Chen, and K.-N. Chen, "Adhesion property of polyimide and passivation layer for polymer/metal wafer-level hybrid bonding in 3D integration," 2018 IEEE 68th Electronic Components and Technology Conference (ECTC), San Diego, CA, pp. 401-406, 29 May 2018-1 June 2018. https://doi.org/10.1109/ectc.2018.00067.

[5] Brigham Young University, "Coefficient of thermal expansion (CTE)." https://cleanroom.byu.edu/cte_materials.

[6] Analog Devices. "High-temperature electronics pose design and reliability challenges," April 2012. https://www.analog.com/en/analog-dialogue/articles/high-temperature-electronic-pose-design-challenges.html.

[7] H. Ardebili, J. Zhang, and M. Pecht, *Encapsulation Technologies for Electronic Applications*, William Andrew, Applied science Publishers, 2nd ed., 2018. https://www.elsevier.com/books/encapsulation-technologies-for-electronic-applications/ardebili/978-0-12-811978-5.

[8] Perkin Elmer, "Dynamic mechanical analysis basics: part 2 thermoplastic transitions and properties." https://resources.perkinelmer.com/lab-solutions/resources/docs/app_thermaldynmechanalybasicspart2.pdf.

[9] R. Subramanian, M.T. Potriger, J.H. Morris, and J.P. Curilla, "Effect of moisture on the physical properties of polyimide films," *MRS Online Proceedings Library*, Vol. 227, No. 1, p. 147, 1991. https://doi.org/10.1557/proc-227-147.

[10] Semiconductor Digest. "Contamination affects the reliability of microelectronics," https://sst.semiconductor-digest.com/1995/05/contamination-affects-the-reliability-of-microelectronics/.

[11] C.A. Yang, J. Wu, C.C. Lee, and C.R. Kao, "Analyses and design for electrochemical migration suppression by alloying indium into silver," *Journal of Materials Science Materials in Electronics*, Vol. 29, No. 16, pp. 13878-13888, 2018. https://doi.org/10.1007/s10854-018-9520-3.

[12] E.L. Lee, A.S.M.A. Haseeb, W.J. Basirun, Y.H. Wong, M.F.M. Sabri, and B.Y. Low, "In-situ study of electrochemical migration of tin in the presence of bromide ion," *Scientific Reports (UK)*, Vol. 11, No. 1, p. 15768, 2021. https://doi.org/10.1038/s41598-021-95276-0.

[13] Medgyes B, Gharaibeh A, Rigler D, Harsányi G, "On the electrochemical migration mechanism of gold in electronics—less reliable than expected?" *Materials (Basel)*. Vol. 14, No. 18, p. 5237, 12 September 2021. https://doi.org/10.3390/ma14185237. PMID: 34576462; PMCID: PMC8465352.

[14] J.J. Steppan, J.A. Roth, L.C. Hall, D.A. Jeannotte, and S.P. Carbone, "A review of corrosion failure mechanisms during accelerated tests: electrolytic metal migration," *Jorunal of the Electrochemical Society*, Vol. 134, No. 1, pp. 175-190, 1987. https://doi.org/10.1149/1.2100401.

[15] B.K. Vaughen, J.A. Roth, J.J. Steppan, L.C. Hall, and C.P. Major, "Electrolytic copper migration in accelerated tests: I. polyethylene glycol-400 doped with ammonium perchlorate," *Journal of the Electrochemical Society*, Vol. 135, No. 8, pp. 2027-2033, 1988. https://doi.org/10.1149/1.2096201.

[16] D. Minzari, M.S. Jellesen, P. Møller, P. Wahlberg, and R. Ambat, "Electrochemical migration on electronic chip resistors in chloride environments," *IEEE Transactions on Device and Materials Reliability*, Vol. 9, No. 3, pp. 392-402, 2009. https://doi.org/10.1109/tdmr.2009.2022631.

[17] P. Yi, K. Xiao, K. Ding, C. Dong, and X. Li, "Electrochemical migration behavior of copper-clad laminate and electroless nickel/immersion gold printed circuit boards under thin electrolyte layers," *Materials (Basel)*, Vol. 10, No. 2, p. 137, 2017. https://doi.org/10.3390/ma10020137.

[18] B. Medgyes, P. Szabó, S. Ádám, L. Tar, M. Ruszinkó, and R. Berényi, "Electrochemical migration of ENIG surface finish in Na_2SO_4 environment," 2018 41st International Spring Seminar on Electron Technology (ISSE), pp. 1–5, Zlatibor, Serbia, 2018. https://doi.org/10.1109/isse.2018.8443622.

[19] M. Töpper, T. Fischer, T. Baumgartner, and H. Reichl, "A comparison of thin film polymers for wafer level packaging," 2010 Proceedings 60th Electronic Components and Technology Conference (ECTC), pp. 769–776, Las Vegas, NV, 2010. https://doi.org/10.1109/ectc.2010.5490751.

[20] M.E. Mills, P. Townsend, D. Castillo, S. Martin, and A. Achen, "Benzocyclobutene (DVS-BCB) polymer as an interlayer dielectric (ILD) material," *Microelectronic Engineering*, Vol. 33, No. 1–4, pp. 327-334, 1997. https://doi.org/10.1016/s0167-9317(96)00061-5.

[21] Y.-H. Kim, J. Kim, G.F. Walker, C. Feger, and S.P. Kowalczyk, "Adhesion and interface investigation of polyimide on metals," *Journal of Adhesion Science and Technology*, Vol. 2, No. 1, pp. 95-105, 1988. https://doi.org.10.1163/156856188x00101.

[22] JEDEC. "Highly accelerated temperature and humidity stress test (HAST)," May 2021. https://www.jedec.org/standards-documents/docs/jesd-22-a110c.

[23] Y.H. Xia, W. Jillek, and E. Schmitt, "In-situ observation on electrochemical migration of lead-free solder joints under water drop test," 2008 International Conference on Electronic Packaging Technology & High Density Packaging, pp. 1–5, Shanghai, China, 2008. https://doi.org/10.1109/icept.2008.4607147.

[24] Y.R. Yoo and Y.S. Kim, "Elucidation of the relationship between the electrochemical migration susceptibility of SnPb solders for PCBs and the composition of the resulting dendrites," *Metals and Materials International*, Vol. 16, No. 4, pp. 613-619, 2010. https://doi.org/10.1007/s12540-010-0814-0.

[25] J.J. Steppan, W.R. Seebaugh, J.A. Roth, and L.C. Hall, "An improved accelerated test chamber for electrolytic metal migration and corrosion," *Jorunal of the Electrochemical Society*, Vol. 132, No. 11, pp. 2567-2571, 1985. https://doi.org/10.1149/1.2113625.

[26] M. Chereches, D. Bejan, E.I. Chereches, A. Alexandru, and A.A. Minea, "An experimental study on electrical conductivity of several oxide nanoparticle enhanced PEG 400 fluid," *International Journal of Thermophysics*, Vol. 42, No. 7, p. 104, 2021. https://doi.org/10.1007/s10765-021-02855-4.

[27] G.I.A. Kumar, J. Alptekin, J. Caperton, A. Salunke, and O. Chyan, "Accelerated reliability testing of Cu-Al bimetallic contact by a micropattern

corrosion testing platform for wire bond device application," *MethodsX*, Vol. 8, p. 101320, 2021. https://doi.org/10.1016/j.mex.2021.101320.

[28] K. Ding, X. Li, K. Xiao, C. Dong, K. Zhang, and R. Zhao, "Electrochemical migration behavior and mechanism of PCB-ImAg and PCB-HASL under adsorbed thin liquid films," *Transactions of Nonferrous Metals Society*, Vol. 25, No. 7, pp. 2446-2457, 2015. https://doi.org/10.1016/s1003-6326(15)63861-4.

[29] J.A. Baird, R. Olayo-Valles, C. Rinaldi, and L.S. Taylor, "Effect of molecular weight, temperature, and additives on the moisture sorption properties of polyethylene glycol," *Journal of Pharmaceutical Sciences*, Vol. 99, No. 1, pp. 154-168, 2010. https://doi.org/10.1002/jps.21808.

[30] J. Soleymani, V. Jouyban-Gharamaleki, E. Kenndler, and A. Jouyban, "Measurement and modeling of sodium chloride solubility in binary mixtures of water + polyethylene glycol 400 at various temperatures," *Journal of Molecular Liquids*, Vol. 316, p. 113777, 2020. https://doi.org/10.1016/j.molliq.2020.113777.

[31] O.M. Chyan and M. Asokan, United States Patent Application US 2021/0071308, 2021. https://patentscope.wipo.int/search/en/detail.jsf?docId=US319904406&docAn=17015046.

[32] M.-S. Hong and J.-G. Kim, "Method for mitigating electrochemical migration on printed circuit boards," *Journal of Electronic Materials*, Vol. 48, No. 8, pp. 5012-5017, 2019. https://doi.org/10.1007/s11664-019-07300-9.